Earthq Eng & Eng Vib (2010) 9: 481-491 **DOI**: 10.1007/s11803-010-0030-4

A modified normalized input-output minimization (Mod-NIOM) method for seismic wave propagation modeling

Santa Man Shrestha[1†], Hideji Kawakami[2‡], Eric Augustus Tingatinga[3§] and Hidenori Mogi[1*]

1. *Department of Civil and Environmental Engineering, Saitama University, Saitama, Japan*
2. *Geosphere Research Institute, Saitama University, Saitama, Japan*
3. *Institute of Civil Engineering, University of the Philippines Diliman, Philippine*

Abstract: A new method for wave propagation modeling is introduced in this paper. By using the constraint optimization (Lagrange multiplier) method, the sum of weighted squared Fourier amplitudes is minimized when subjected to a constraint. The sum of the maximum amplitudes obtained from all output models is normalized to unity and is taken as a constraint. In this method, all the actual time histories are considered as outputs and dealt with equally. Independently of the combinations of time histories (or the first time history selected) during the analysis, the method captures the relationship of actual time histories by showing clear peaks. This paper describes the formulation of the models and illustrates the advantage of this method over the normalized input-output minimization (NIOM) method. The Mod-NIOM is then used to analyze the time histories of the Hyogoken-nanbu earthquake recorded at the Port Island vertical array site in Kobe, which suffered from liquefaction caused by the strong motions during the main shock. This method showed good correlations between the observed time histories at the site even though the surface time history was greatly modified by the liquefaction.

Keywords: wave propagation; constraint optimization; S-wave velocity; liquefaction; amplification; vertical array; Hyogoken-nanbu earthquake

1 Introduction

Seismic waves carry large amounts of information about their source, the physical properties of their propagation path, and local site conditions. Data recorded by seismometers can be used to quantitatively analyze the mechanisms, locations, and magnitudes of earthquakes as well as to investigate stratified ground structures and physical properties of a site for engineering purposes. Several methods have been proposed to analyze the wave propagation (Bendat and Piersol, 1971; Harichandran and Vanmarcke 1986; Kawakami and Haddadi, 1998; Kramer, 1996; Thomson and Dahleh, 1992).

The normalized input-output minimization (NIOM) (Kawakami and Haddadi, 1998) is a numerical modeling method. By using the constraint optimization technique, it allows simple relationships between the observed time histories to be obtained in layers. In this method, one observed time history is taken to be the input while others are taken to be outputs; hence, the input and outputs are not dealt with equally. The input model is subjected to a constraint, and its maximum amplitude is normalized to unity. For this reason, the input model is always similar to a symmetrical single pulse. Therefore, the time history observed at the ground surface is always selected as the input observed time history. In fact, the time histories at a given depth consist of multiple waves containing incident and reflected waves, so the NIOM method is not applicable when the input time history is taken at a depth other than that at the ground surface.

This paper describes a new method for wave propagation analysis, called the modified normalized input-output minimization (Mod-NIOM). This method can correlate different time histories observed at an array, independent of the selection of the first time history (the 'input' in the NIOM method). In this method, a simple pulse is considered to be the input time history, and all the observed time histories are considered as outputs and are dealt with equally. Since all the outputs are dealt with equally, this method provides a more rational relationship between them. Consequently, the result doesn't depend on whether the first output (first time history) of the analysis is at the surface or at a given depth. Hence, this new method can compare the amplitudes of any of the observed time histories with others, enabling the arrival times of the incident and reflected waves as well as

Correspondence to: Santa Man Shrestha, Department of Civil and Environmental Engineering, Saitama University, 255 Shimo-okubo, Sakura-ku, Saitama-shi, Saitama 338-8570, Japan
Tel: +81-80-3344-7266
E-mail: s07de056@mail.saitama-u.ac.jp
[†]PhD candidate; [‡]Professor; [§]Assistant Professor; *Associate Professor

Received March 9, 2010; **Accepted** August 11, 2010

relative amplitudes of their peaks to be obtained.

In this paper, the advantages of Mod-NIOM over NIOM are demonstrated in a simulated data analysis. To illustrate the proposed Mod-NIOM method, records from the main shock and some aftershocks of the Hyogoken-nanbu earthquake at the Port Island vertical array site are analyzed. Several studies (Aguirre and Irikura, 1997; Haddadi and Kawakami, 1998) showed that a large reduction in the S-wave velocities occurred in the surface layer of the Port Island site during the main shock of the Hyogoken-nanbu earthquake, and this reduction was due to surface liquefaction. After the main shock, the S-wave velocity in this layer increased as a result of recovery of the soil. In this paper, the obtained S-wave velocities are compared with the S-wave velocities calculated from down-hole measurements.

2 Methodology

For linear systems subjected to an input motion, the input motion $f(t)$ and outputs $g_l(t)$, (l = 1,...,P) can be related by means of the convolution principle as

$$g_l(t)=\int_{-\infty}^{+\infty} h_l(\tau)\,f(t-\tau)\,\mathrm{d}\tau \tag{1}$$

where $h_l(\tau)$ is the impulse response functions.

Similarly, these input-outputs in the frequency domain can be related by transfer functions $H_l(\omega)$as

$$G_l(\omega_i)=H_l(\omega_i)F(\omega_i),\quad \left(i=0,...,N-1 \quad \text{and} \quad \omega_i=\frac{2\pi}{N\Delta t}i\right) \tag{2}$$

where $F(\omega_i)$ and $G_l(\omega_i)$ represent the input and different outputs of the actual ground motion records in the frequency domain, Δt is the sampling rate in the time domain, and N is the total number of samples. Similarly, l = 1,...,P, where P is the total number of observed time histories considered as outputs. In the Mod-NIOM method, a simple pulse is always considered as the input (i.e., $F(\omega_i)$ = constant), and all the actual time histories are considered as outputs $G_l(\omega_i)$.

Let $Y_0(\omega_i)$ be the input model and $Y_l(\omega_i)$, (l = 1,...,P) be the output models in the Mod-NIOM method. As $Y_0(\omega_i)$ and $Y_l(\omega_i)$ are numerical models of $F(\omega_i)$ and $G_l(\omega_i)$, the transfer functions from the actual system should be the same as those between the corresponding input-output models. Hence

$$Y_l(\omega_i)=H_l(\omega_i)Y_0(\omega_i) \tag{3}$$

The inverse discrete Fourier transform of the model can in general be written as

$$y(m\Delta t)=\frac{1}{N\Delta t}\sum_{i=0}^{N-1}Y(\omega_i)\mathrm{e}^{\frac{\mathrm{j}2\pi im}{N}},\quad \mathrm{j}=\sqrt{-1} \tag{4}$$

The constraint optimization (Lagrange multiplier) method is used in the formulation of the input-output models, and the Lagrange function (L) can be formulated in the following two steps:

Step 1: Formulate an objective function, with variables of the input and output models

The squared Fourier amplitudes of the input-output models and their derivatives are properly weighted. The derivatives of the Fourier amplitudes are used to examine the wave propagation of different frequency contents and to change the spectrum of the models. The sum of these weighted squared Fourier amplitudes is taken to be an objective function (let D) with variables of the input model ($Y_0(\omega_i)$) and output models ($Y_l(\omega_i)$), i.e.,

$$D=\sum_{i=0}^{N-1}\left[c_0\left|Y_0(\omega_i)\right|^2+k_0\omega_i^2\left|Y_0(\omega_i)\right|^2+\sum_{l=1}^{P}\left\{c_l\left|Y_l(\omega_i)\right|^2+k_l\omega_i^2\left|Y_l(\omega_i)\right|^2\right\}\right] \tag{5}$$

where, $c_0,...,c_P$ are the weighting constants for the squared Fourier amplitudes and $k_0,...,k_P$ are the weighting constants for the derivatives of the Fourier amplitudes. The contribution of the frequency components is controlled by the weighting constants k_0 and k_l, (l = 1,...,P).

Step 2: Develop the constraint

The sum of amplitudes of the first output model $y_1(t)$ at t_{m1} = 0 s and the rest of the output models $y_l(t)$ at other times $t_{m_l}=m_l\Delta t$ (where l=2,...,P) are normalized to unity, which gives

$$y_1(0)+\sum_{l=2}^{P}y_l(t_{m_l})=1 \tag{6}$$

Equation (6) does not have any physical meaning. It is only a condition that allows normalized amplitudes of the peaks in output models to be obtained at particular times in the result. This makes it easier to determine the relative amplitudes of the peaks among the outputs in the analysis results. Since the peak of the first output model is to appear at 0 s, the relative times of the peaks of other output models can be easily read with this reference. Transforming Eq. (6) into the frequency domain and rearranging gives

$$\frac{1}{N\Delta t}\sum_{i=0}^{N-1}\left\{Y_1(\omega_i)+\sum_{l=2}^{P}Y_l(\omega_i)\mathrm{e}^{\frac{\mathrm{j}2\pi im_l}{N}}\right\}=1 \tag{7}$$

Equation (7) is a constraint for optimizing the objective function of Eq. (5).

Accordingly, the Lagrange function (L) can be written for D (i.e., Eq. (5)) subject to the constraint of Eq. (7) as

$$L=D-\lambda\left[\frac{1}{N\Delta t}\sum_{i=0}^{N-1}\left\{Y_1(\omega_i)+\sum_{l=2}^{P}Y_l(\omega_i)\mathrm{e}^{\frac{\mathrm{j}2\pi im_l}{N}}\right\}-1\right] \tag{8}$$

where λ is the Lagrange multiplier. Substituting the value of D from Eq. (5) into Eq.(8) yields

$$L=\sum_{i=0}^{N-1}\Big[c_0\left|Y_0(\omega_i)\right|^2+k_0\omega_i^2\left|Y_0(\omega_i)\right|^2+\sum_{l=1}^{P}\left\{c_l\left|Y_l(\omega_i)\right|^2+k_l\omega_i^2\left|Y_l(\omega_i)\right|^2\right\}\Big]-\lambda\left[\frac{1}{N\Delta t}\sum_{i=0}^{N-1}\left\{Y_1(\omega_i)+\sum_{l=2}^{P}Y_l(\omega_i)\,\mathrm{e}^{\frac{\mathrm{j}2\pi im_l}{N}}\right\}-1\right] \quad (9)$$

Substituting Eq. (3) into Eq. (9) and rearranging, gives

$$L=\sum_{i=0}^{N-1}\Big[\left(c_0+k_0\omega_i^2\right)Y_0(\omega_i)Y_0^*(\omega_i)+\sum_{l=1}^{P}\left(c_l+k_l\omega_i^2\right)\left|H_l(\omega_i)\right|^2Y_0(\omega_i)Y_0^*(\omega_i)\Big]-\lambda\left[\frac{1}{N\Delta t}\sum_{i=0}^{N-1}\left\{H_1(\omega_i)+\sum_{l=2}^{P}H_l(\omega_i)\,\mathrm{e}^{\frac{\mathrm{j}2\pi im_l}{N}}\right\}Y_0(\omega_i)-1\right] \quad (10)$$

where $Y_0(\omega_i)$ and $Y_0^*(\omega_i)$ are complex conjugate pairs. Taking the same relationship of weighting constants for input and output as $k_0/c_0=\ldots\ldots=k_l/c_l=\ldots\ldots=k_P/c_P$ gives

$$L=\sum_{i=0}^{N-1}\left[\left\{c_0+\sum_{l=1}^{P}c_l\left|H_l(\omega_i)\right|^2\right\}\left(1+\frac{k_0}{c_0}\omega_i^2\right)Y_0(\omega_i)Y_0^*(\omega_i)\right]-\lambda\left[\frac{1}{N\Delta t}\sum_{i=0}^{N-1}\left\{H_1(\omega_i)+\sum_{l=2}^{P}H_l(\omega_i)\,\mathrm{e}^{\frac{\mathrm{j}2\pi im_l}{N}}\right\}Y_0(\omega_i)-1\right] \quad (11)$$

Expanding the terms of Eq. (11) for $i = 0$,

$$1\le i\le\left(\frac{N}{2}-1\right),\ i=\frac{N}{2}\ \text{and}\ \left(\frac{N}{2}+1\right)\le i\le(N-1),$$

converting the expanded terms by using the properties of DFT for real $y(t)$ (i.e., $Y(\omega_{i+N})=Y(\omega_i)$ and $Y(\omega_{N-i})=Y^*(\omega_i)$), and rearranging the terms gives

$$L=\left(c_0+\sum_{l=1}^{P}c_l\left|H_l(\omega_0)\right|^2\right)\left(1+\frac{k_0}{c_0}\omega_0^2\right)Y_0(\omega_0)Y_0^*(\omega_0)+2\sum_{i=1}^{\frac{N}{2}-1}\left[\left(c_0+\sum_{l=1}^{P}c_l\left|H_l(\omega_i)\right|^2\right)\left(1+\frac{k_0}{c_0}\omega_i^2\right)Y_0(\omega_i)Y_0^*(\omega_i)\right]+\left(c_0+\sum_{l=1}^{P}c_l\left|H_l\left(\omega_{\frac{N}{2}}\right)\right|^2\right)\left(1+\frac{k_0}{c_0}\omega_{\frac{N}{2}}^2\right)Y_0\left(\omega_{\frac{N}{2}}\right)Y_0^*\left(\omega_{\frac{N}{2}}\right)-\frac{\lambda}{N\Delta t}\left(H_1(\omega_0)+\sum_{l=2}^{P}H_l(\omega_0)\right)Y_0(\omega_0)-\frac{\lambda}{N\Delta t}\sum_{i=1}^{\frac{N}{2}-1}\left(H_1(\omega_i)+\sum_{l=2}^{P}H_l(\omega_i)\,\mathrm{e}^{\frac{\mathrm{j}2\pi im_l}{N}}\right)Y_0(\omega_i)-\frac{\lambda}{N\Delta t}\left(H_1\left(\omega_{\frac{N}{2}}\right)+\sum_{l=2}^{P}H_l\left(\omega_{\frac{N}{2}}\right)\mathrm{e}^{\mathrm{j}\pi m_l}\right)Y_0\left(\omega_{\frac{N}{2}}\right)-\frac{\lambda}{N\Delta t}\sum_{i=1}^{\frac{N}{2}-1}\left(H_1^*(\omega_i)+\sum_{l=2}^{P}H_l^*(\omega_i)\,\mathrm{e}^{\frac{-\mathrm{j}2\pi im_l}{N}}\right)Y_0^*(\omega_i)+\lambda. \quad (12)$$

In Eq. (12), Y and Y^* are the complex conjugates, so the value of L may be regarded as a function of Y and Y^*. The minimum condition can simply be expressed as (Claerbout, 1985)

$$\frac{\partial L}{\partial Y}=\frac{\partial L}{\partial Y^*}=0 \quad (13)$$

Therefore, minimizing L from Eq. (12) as $\frac{\partial L}{\partial Y_0(\omega_i)}=0$ yields

$$Y_0^*(\omega_i)=\frac{\lambda}{2N\Delta t}\left[\frac{H_1(\omega_i)+\sum_{l=2}^{P}H_l(\omega_i)\,\mathrm{e}^{\frac{\mathrm{j}2\pi im_l}{N}}}{\left\{c_0+\sum_{l=1}^{P}c_l\left|H_l(\omega_i)\right|^2\right\}\left(1+\frac{k_0}{c_0}\omega_i^2\right)}\right] \quad (14)$$

and $\frac{\partial L}{\partial Y_0^*(\omega_i)}=0$ yields

$$Y_0(\omega_i)=\frac{\lambda}{2N\Delta t}\left[\frac{H_1^*(\omega_i)+\sum_{l=2}^{P}H_l^*(\omega_i)\,\mathrm{e}^{\frac{-\mathrm{j}2\pi im_l}{N}}}{\left\{c_0+\sum_{l=1}^{P}c_l\left|H_l(\omega_i)\right|^2\right\}\left(1+\frac{k_0}{c_0}\omega_i^2\right)}\right] \quad (15)$$

Similarly, $\frac{\partial L}{\partial\lambda}=0$ yields

$$\frac{1}{N\Delta t}\sum_{i=0}^{N-1}\left\{H_1(\omega_i)+\sum_{l=2}^{P}H_l(\omega_i)\,\mathrm{e}^{\frac{\mathrm{j}2\pi im_l}{N}}\right\}Y_0(\omega_i)-1=0 \quad (16)$$

Solving Eq. (15) and Eq. (16), gives

$$\lambda = 2(N\Delta t)^2 \frac{1}{\sum_{i=0}^{N-1}\left[\frac{\left(H_1(\omega_i)+\sum_{l=2}^{P}H_l(\omega_i)\,e^{\frac{j2\pi im_l}{N}}\right)\left(H_1^*(\omega_i)+\sum_{l=2}^{P}H_l^*(\omega_i)\,e^{\frac{-j2\pi im_l}{N}}\right)}{\left(c_0+\sum_{l=1}^{P}c_l\left|H_l(\omega_i)\right|^2\right)\left(1+\frac{k_0}{c_0}\omega_i^2\right)}\right]} \tag{17}$$

Substituting the values of $Y_0^*(\omega_i)$, $Y_0(\omega_i)$ and λ from Eqs. (14), (15) and (17), respectively, into Eq. (11) and solving give

$$L = (N\Delta t)^2 \frac{1}{\sum_{i=0}^{N-1}\left[\frac{\left\{H_1(\omega_i)+\sum_{l=2}^{P}H_l(\omega_i)\,e^{\frac{j2\pi im_l}{N}}\right\}\left\{H_1^*(\omega_i)+\sum_{l=2}^{P}H_l^*(\omega_i)\,e^{\frac{-j2\pi im_l}{N}}\right\}}{\left\{c_0+\sum_{l=1}^{P}c_l\left|H_l(\omega_i)\right|^2\right\}\left(1+\frac{k_0}{c_0}\omega_i^2\right)}\right]}. \tag{18}$$

From Eq. (18), the optimum value of L is found for different values of m_2, m_3,...,m_P. Then the simplified input model is

$$Y_0(\omega_i) = \left[\frac{N\Delta t\left\{H_1^*(\omega_i)+\sum_{l=2}^{P}H_l^*(\omega_i)\,e^{\frac{-j2\pi im_l}{N}}\right\}}{\left\{c_0+\sum_{l=1}^{P}c_l\left|H_l(\omega_i)\right|^2\right\}\left(1+\frac{k_0}{c_0}\omega_i^2\right)}\right]\frac{1}{A} \tag{19}$$

and the output models are

$$Y_l(\omega_i) = H_l(\omega_i)\left[\frac{N\Delta t\left\{H_1^*(\omega_i)+\sum_{l=2}^{P}H_l^*(\omega_i)\,e^{\frac{-j2\pi im_l}{N}}\right\}}{\left\{c_0+\sum_{l=1}^{P}c_l\left|H_l(\omega_i)\right|^2\right\}\left(1+\frac{k_0}{c_0}\omega_i^2\right)}\right]\frac{1}{A}, \tag{20}$$

where

$$A = \sum_{i=0}^{N-1}\left[\frac{\left\{H_1(\omega_i)+\sum_{l=2}^{P}H_l(\omega_i)\,e^{\frac{j2\pi im_l}{N}}\right\}\left\{H_1^*(\omega_i)+\sum_{l=2}^{P}H_l^*(\omega_i)\,e^{\frac{-j2\pi im_l}{N}}\right\}}{\left\{c_0+\sum_{l=1}^{P}c_l\left|H_l(\omega_i)\right|^2\right\}\left(1+\frac{k_0}{c_0}\omega_i^2\right)}\right].$$

The values of the transfer functions, $H_l(\omega_i), (l=1,...,P)$, in the input and output models of Eqs. (19) and (20) are calculated from the observed input and output time histories. Equation (20) gives the output models in the frequency domain. The inverse Fourier transforms of these equations gave the simplified output models in the time domain. In this way, the simplified models of complicated actual ground motions are obtained.

3 Verification of the proposed Mod-NIOM and comparison to NIOM by analyzing simple simulated time histories

The models were tested and verified by analyzing simple simulated time histories. Five simulated time histories at SD1–SD5 are generated as shown in Fig. 1. The first one at SD1 is a single wave plus a white noise, $n_1(t)$. All of the others at SD2–SD5 are generated with successive shifts to some time with different amplitude, and adds, besides a white noise, $n_i(t)$, $(i=1,...,5)$ is added as for the first one, and hence, the equations at SD1–SD5 are

SD1: $$f_1(t) = 1.0 f_0(t) + n_1(t) \tag{21a}$$

SD2: $$f_2(t) = 0.5 f_0(t+0.15) + 0.5 f_0(t-0.15) + n_2(t) \tag{21b}$$

SD3: $$f_3(t) = 0.5 f_0(t+0.30) + 0.5 f_0(t-0.30) + n_3(t) \tag{21c}$$

SD4: $$f_4(t) = 0.5 f_0(t+0.50) + 0.5 f_0(t-0.50) + n_4(t) \tag{21d}$$

SD5: $$f_5(t) = 0.5 f_0(t+0.60) + 0.5 f_0(t-0.60) + n_5(t) \tag{21e}$$

These simulated time histories are shown in Fig. 1. Three types of simulated data combinations, i.e., SD1–SD5, SD2–SD5 and SD3–SD5, were assumed for the analysis. The simulated data combinations were analyzed by both NIOM and Mod-NIOM methods with weighting coefficients of c_0= 1, k_0=0.001 and c_1 = 1, ($l \geq 1$). The Mod-NIOM and NIOM results are shown in Fig. 2. The simple peaks correspond to the arrival times (shifting times) of the simulated waves. In all three combinations, the first data considered ('first output time history' in the Mod-NIOM method and 'input time history' in the NIOM method) are different. In the first combination (i.e. SD1–SD5), the first data considered for the analysis is a single wave (i.e., SD1). Whereas in the other two combinations (i.e., SD2–SD5 and SD3–

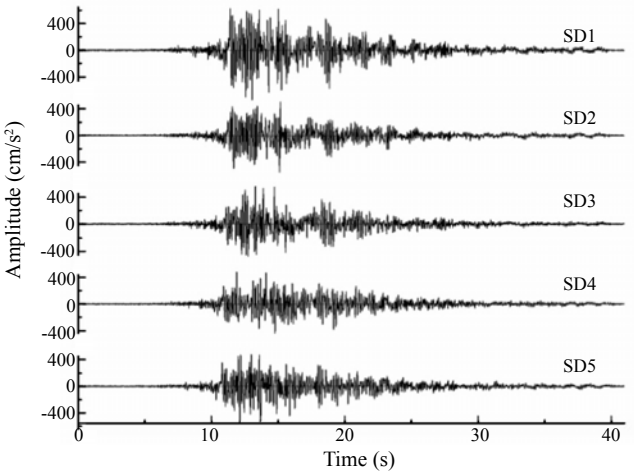

Fig. 1 Simulated time histories

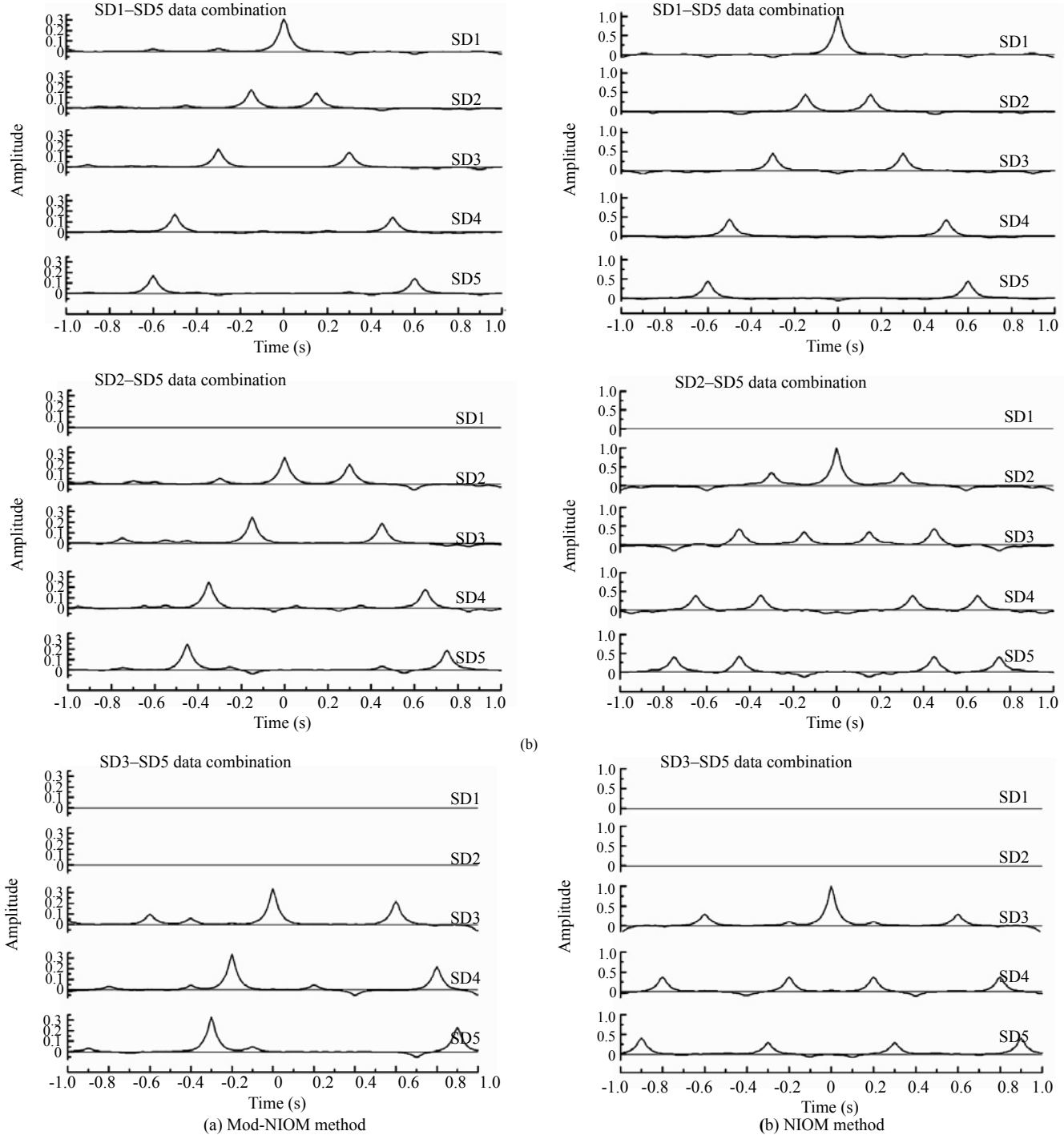

Fig. 2 Analysis results from three different combinations of the simulated data

SD5), the first data considered are combined waves. In Fig. 2(a), the shifting times of each output model are the same in all three combinations. These times are the same as the shifting times used in Eqs. (21a)–(21e). These results show that the Mod-NIOM results are independent of the first data chosen in the analysis. The results of each combination are different in the case of NIOM. The results of the SD1–SD5 combination for both methods (shown in the first row of Figs. 2(a) and 2(b)) are the same because the single wave (SD1) is chosen as the first time history. For other combinations in which the first data considered are symmetrical and combined waves, the NIOM results (Fig. 2(b)) are more complicated than those of the Mod-NIOM. These results demonstrate that Mod-NIOM is more effective than the NIOM method.

In Fig. 2(a), the amplitudes of the peaks obtained for each data combination are different because of the constraint (Eq. (7)) on the formulation of models. The amplitudes in output models increase as the number of output time histories decreases. However, the relative

amplitudes are similar. Therefore, the Mod-NIOM method is capable of analyzing the time histories independently of the data combination (or the first data chosen) in the analysis. The shifting time (the propagation time) between the time histories are easily obtained by reading the times of simple peaks in the output models. Similarly, the relative peak amplitudes are similar to the relative amplitude of the actual simulated time histories.

4 Application to actual ground motion records

4.1 Description of ground motion records and their combinations

The proposed method was used to analyze the Hyogoken-nanbu earthquake of January 17, 1995 at the Port Island vertical array site. Surface liquefaction occurred at Port Island (reclaimed land area) during the main shock of the Hyogoken-nanbu earthquake. The vertical array site is located at the northwest corner of Port Island, near Kobe city. The seismometers were installed at the site at depths of 0 m, 16 m, 32 m and 83 m from the ground surface. Mod-NIOM was used to analyze the time history of the main shock (Fig. 3) and several aftershocks. The soil profile and other relevant soil properties at the Port Island site are given in Table 1 (Department of Urban Development, Kobe city, 1995). The Mod-NIOM analysis was carried out for each earthquake with three different combinations of data. The combinations of data were -

(1) 1st combination: Data at all four seismometers (from 0-83 m levels) with the first output model at 0 m (surface)

(2) 2nd combination: Data at three seismometers (from 16-83 m levels) with the first output model at 16 m

(3) 3rd combination: Data at two seismometers (from 32-83 m levels) with the first output model at 32 m.

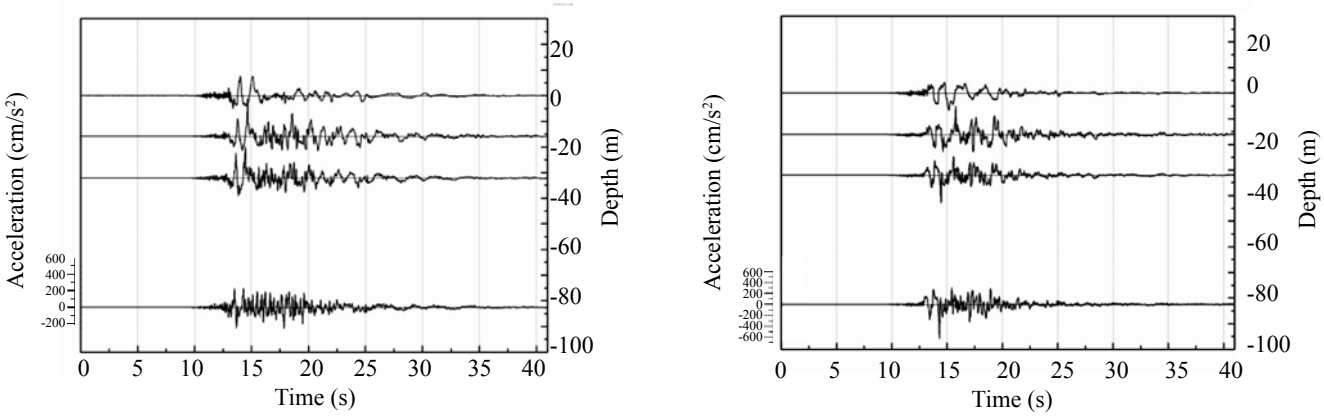

(a) EW components (b) NS components

Fig. 3 Time histories of horizontal components at different depths of the main shock of the Hyogoken-nanbu earthquake (January 17, 1995) recorded at Port Island Vertical Array site (Department of Urban Development, Kobe City, 1995)

Table 1 Soil profile and other relevant soil properties at the Port Island site (Department of Urban Development, Kobe City, 1995)

Depth (m)	Soil type		P- velocity (km/s)	S- velocity (km/s)	Poisson's ratio	Location of seismometer (m)
0 – 2.0	Sandy gravel	Reclaimed	0.26	0.17	0.13	GL-0.0
2.0 – 5.0	Sandy gravel		0.33		0.32	
5.0 – 12.6	Sandy gravel		0.78	0.21	0.46	
12.6 – 19.0	Sand with gravel		1.48	0.21	0.49	GL-16.0
19.0 – 27.0	Alluvial clay		1.18	0.18	0.49	
27.0 – 33.0	Diluvial sand	Sand and clay inter-layered stratum	1.33	0.25	0.48	GL-32.0
33.0 – 50.0	Sand with gravel		1.53	0.31	0.48	
50.0 – 61.0	Diluvial sand		1.61	0.35	0.48	
61.0 – 79.0	Diluvial clay		1.61	0.30	0.48	
79.0 – 85.0	Sand with gravel		2.00	0.32	0.49	GL-83.0

4.2 Results and discussion

Figures 4(a) and 4(b) show the analysis results of the EW and NS components, respectively, of the main shock of the Hyogoken-nanbu earthquake. The first, second and third rows , show the results of 1st, 2nd and 3rd combinations of data, respectively, as stated in Section 4.1. The clear peaks correspond to the arrival times of the S-wave. Moreover, the results in Figs. 4(a) and 4(b) clearly show that the wave propagation times in each layer are the same for all three data combinations. The S-wave propagation times obtained from the Mod-NIOM method and down-hole measurements are tabulated in Table 2. These results show that the S-wave arrival times are the same in the base layer. In the top layer, the propagation time obtained from the Mod-NIOM method is much longer than the arrival time determined from the down-hole measurements.

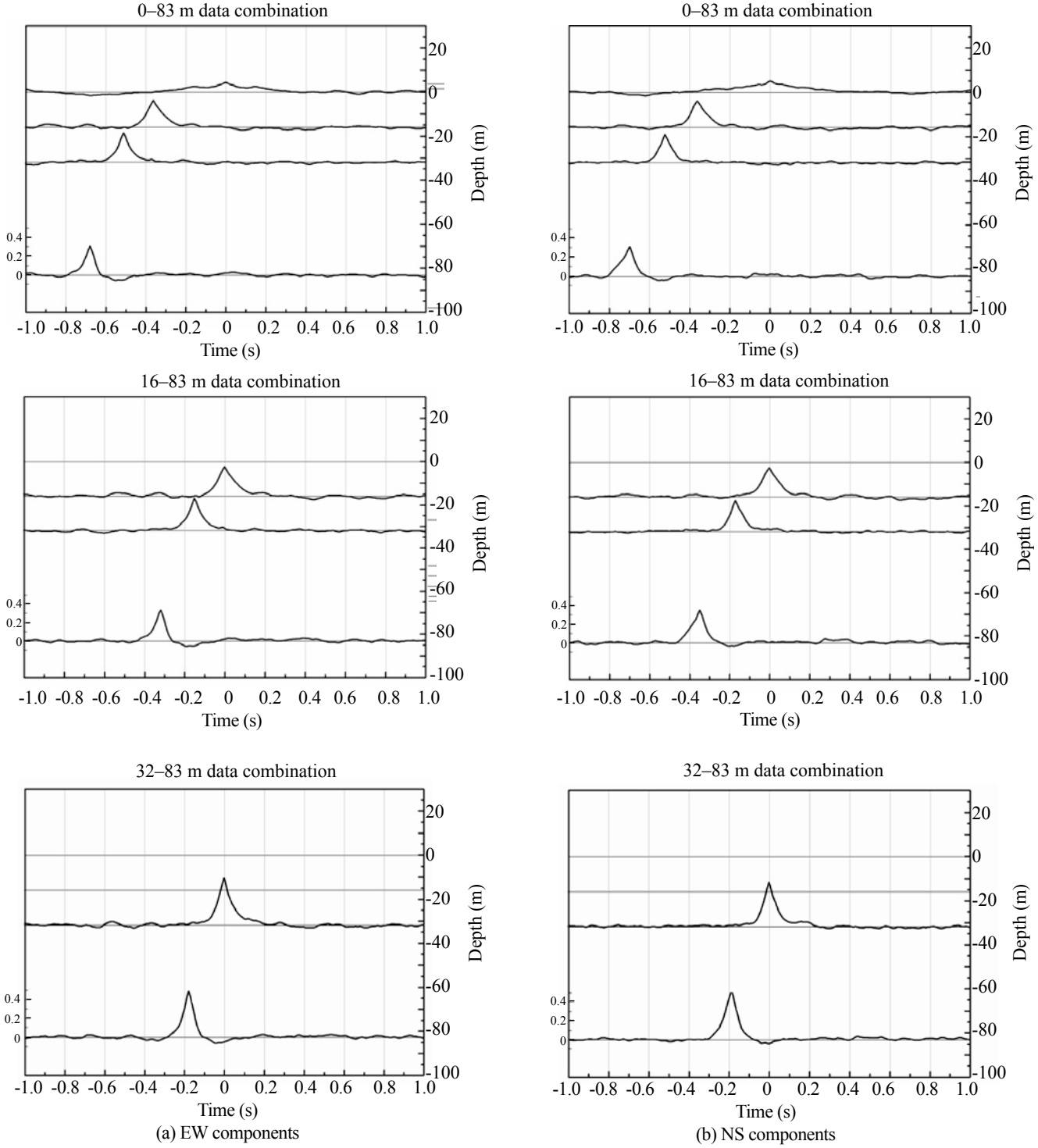

Fig. 4 Mod-NIOM results for the main shock of the Hyogoken-nanbu earthquake. The top, the middle and the bottom show results for 1st, 2nd and 3rd combinations of data

Table 2 Comparison of S-wave propagation times obtained from Mod-NIOM method and down-hole measurements

Layer	S-wave propagation times	
	Mod-NIOM method (s)	Down-hole measurements (s)
Top (0–16 m)	0.36	0.081
Intermediate (16–32 m)	0.15	0.078
Base (32–83 m)	0.17	0.169

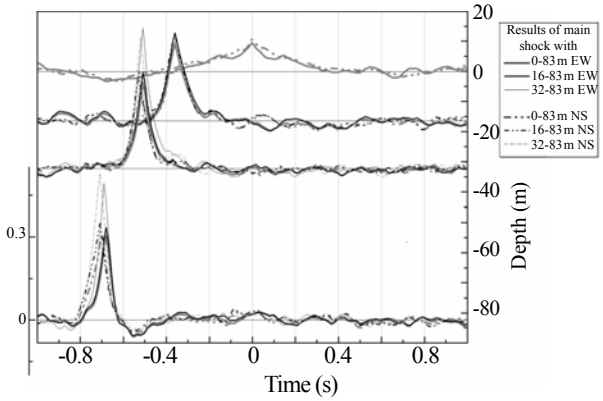

Fig. 5 Analysis results of horizontal components of the main shock plotted together for different data combinations

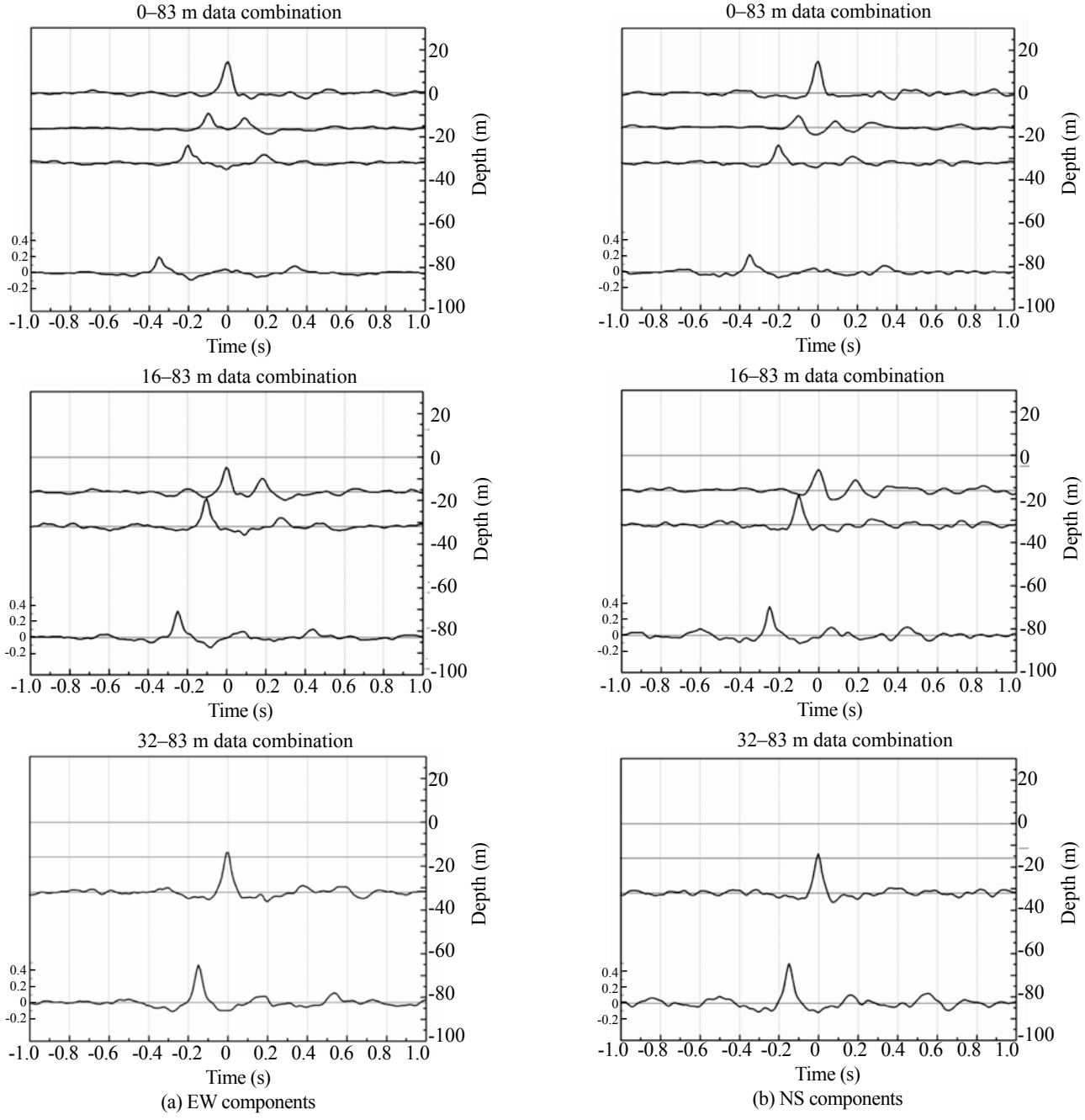

Fig. 6 Mod-NIOM results for the earthquake on March 5, 1995. The top, the middle, and the bottom show results for 1st, 2nd and 3rd combinations of data

To examine the reflected peaks, the analysis results of the horizontal components of the main shock for all three combinations of data are superposed together in Fig. 5. Left hand ordinates represent the relative amplitudes of the output models which were normalized to unity (Figs. 4–8). Note that the relative amplitudes of the output models at the surface are significantly lower than those at the depths (as seen in the results of the 1st combination). The small amplitude at the surface and long S-wave propagation time in the top layer are due to the increase in damping and reduction of soil stiffness during liquefaction of the surface soil. Similarly, the reflected peaks from the ground surface are not traceable in Fig. 5.

Figure 6 shows the results for the EW and NS components of March 5, 1995 earthquake. Similarly Fig. 7 shows the results for the EW and NS components of the three aftershocks on June 19, September 12, and December 27, 1995. Note that a decrease in the S-wave arrival times in the top layer and an increase in the peak amplitudes at the surface can be observed as compared to the results of the main shock. These results indicate a recovery of the soil stiffness after the liquefaction. After the recovery, the damping in the soil decreased

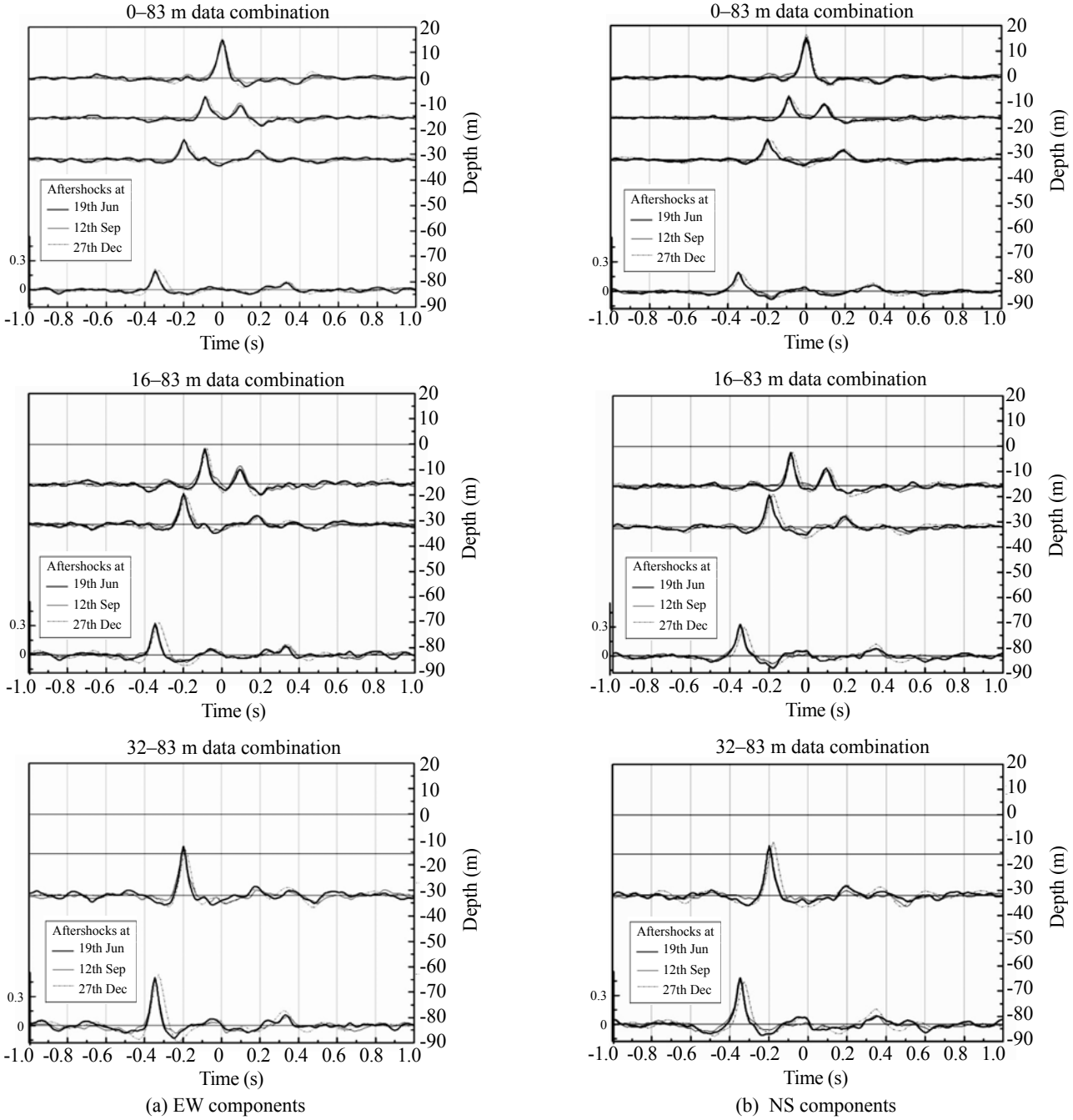

Fig. 7 Mod-NIOM results for three aftershocks on June 19, September 12 and December 27, 1995. The top, the middle and the bottom show results for 1st, 2nd and 3rd combinations of data

and hence the reflected waves can be expected in the downward direction. In Figs. 6 and 7, the reflected peaks from the surface are clearly visible in all combinations of data.

Figure 8 shows the average results of EW and NS components of the main shock and the average results of the EW and NS components of four aftershocks plotted together for different combinations of data. This figure clearly illustrates the difference in arrival times as well as the relative amplitudes of the main shock and aftershocks. The decrease in arrival times in the top layer and increase in the relative amplitude at the surface in the aftershock results are indications of recovery of the liquefied layer.

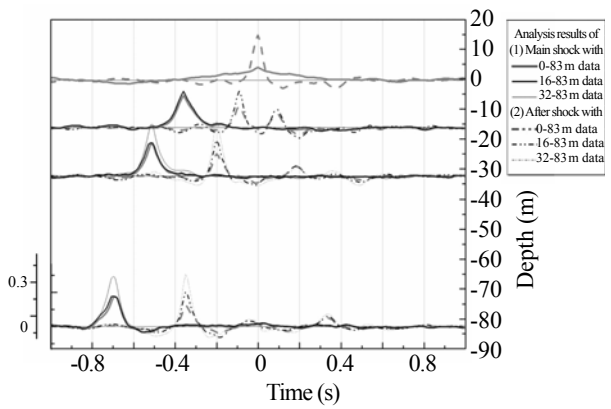

Fig. 8 Averaged results of EW and NS components of the main shock (solid lines) and those of four aftershocks (broken lines) for different data combinations

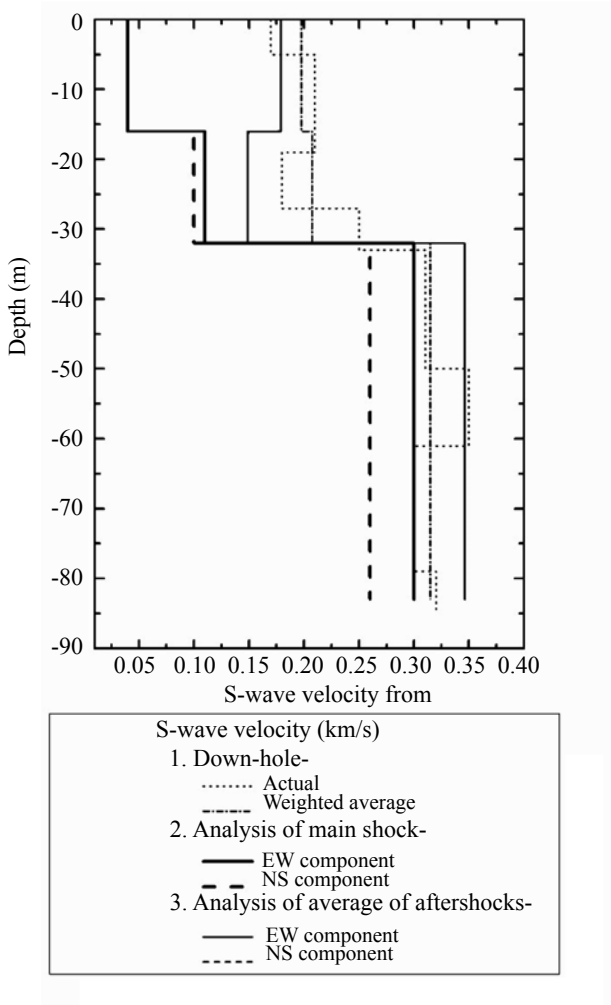

Fig. 9 Comparison of S-wave velocities obtained from analysis of the horizontal components of the main shock and the aftershocks and those from the down-hole measurements. The average results of EW and NS components of the aftershocks have the same S-wave velocities for each layer

Figure 9 compares the S-wave velocities obtained from the Mod-NIOM analysis and those obtained from the down-hole measurements. Note that the S-wave velocity in the top layer, as obtained from the analysis of the main shock, is much less than the value obtained from the down-hole measurements. This reduction of the S-wave velocity is associated with the non-linearity observed in the surface layer due to liquefaction, as shown by other researchers (Aguirre and Irikura, 1997; Haddadi and Kawakami, 1998). Figure 9 also shows an increase in the S-wave velocities in this layer for the aftershocks.

5 Conclusions

A new simplified numerical modeling method for wave propagation analysis was developed. The analysis results of an earthquake event with different combinations of data show that the propagation time in any particular layer is the same for all combinations. Therefore, this method is capable of correlating different observed time histories independently of the combinations of data (or the first output data chosen) in the analysis.

The results for the Port Island site clearly show an increase in the S-wave propagation time in the top layer and a decrease in peak amplitude at the ground surface during the main shock as a result of surface liquefaction. Hence, the reflected peaks in the downward direction from the ground surface are not visible during the main shock.

The results of the aftershocks at the same site show a decrease in the S-wave propagation time in the top layer and an increase in the peak amplitude at the surface as compared to the results of the main shock. These results indicate the recovery of the soil. Hence, the reflected peaks from the ground surface are clearly visible in all the aftershocks.

Acknowledgement

The authors would like to thank the Department of Urban Development, Kobe City for providing the earthquake observation records from the Port Island vertical array site.

References

Aguirre J and Irikura K (1997), "Nonlinearity,

Liquefaction, and Velocity Variation of Soft Soil Layers in Port Island, Kobe, during the Hyogo-ken Nanbu Earthquake," *Bulletin of the Seismological society of America*, **87**(5): 1244–1258.

Bendat JS and Piersol AG (1971), *Random Data: Analysis and Measurement Procedures*, John Wiley & Sons.

Claerbout JF (1985), *Fundamentals of Geophysical Data Processing*, Blackwell Scientific Publications.

Department of Urban Development, Kobe City (1995), *Report on ground deformation of reclaimed land due to Kobe earthquake.* (in Japanese).

Haddadi HR and Kawakami H (1998), "Effect of Liquefaction on Ground Motion During the Hyogoken-nanbu Earthquake, 1995, in Japan by Using NIOM Method," *The Effects of Surface Geology on Seismic Motion*, Irikura, Kudo, Okada & Sasatani (eds), Balkema, Rotterdam, **2**: 1015–1022.

Harichandran RS and Vanmarcke EH (1986), "Stochastic Variation of Earthquake Ground Motions in Space and Time," *Journal of Engineering Mechanics*, ASCE, **112**(2): 154 –174.

Kawakami H and Haddadi HR (1998), "Modeling Wave Propagation by Using Normalized Input-output Minimization (NIOM)," *Soil Dynamics and Earthquake Engineering*, **17**: 117–126.

Kramer SL (1996), *Geotechnical Earthquake Engineering*, Prentice Hall, New Jersey.

Thomson WT and Dahleh MD (1992), *Theory of Vibration with Applications,* Prentice Hall, New Jersey.